Thermal Decomposition Synthesis of Iron Oxide Nanoparticles with Diminished Magnetic Dead Layer by Controlled Addition of Oxygen

Mythreyi Unni,[†] Amanda M. Uhl,[‡] Shehaab Savliwala,[†] Benjamin H Savitzky,[£] Rohan Dhavalikar,[†] Nicolas Garraud,[||] David P Arnold,[||] Lena F. Kourkoutis, [#,δ] Jennifer S. Andrew,[‡] and Carlos Rinaldi[†,§]*

[†]Department of Chemical Engineering, University of Florida, Gainesville, FL, 32611, USA
[‡]Department of Materials Science and Engineering, University of Florida, Gainesville, FL, 32611, USA [£]Department of Physics, Cornell University, Ithaca, NY, 14853, USA
[#]Applied & Engineering Physics, Cornell University, Ithaca, NY, 14853, USA
[δ]Kavli Institute at Cornell for Nanoscale Science, Cornell University, Ithaca, NY, 14853, USA
|| Interdisciplinary Microsystems Group, Department of Electrical and Computer Engineering, University of Florida, Gainesville, FL, 32611, USA [§]J. Crayton Pruitt Family Department of Biomedical Engineering, University of Florida, Gainesville, FL, 32611, USA

I. Supporting Results

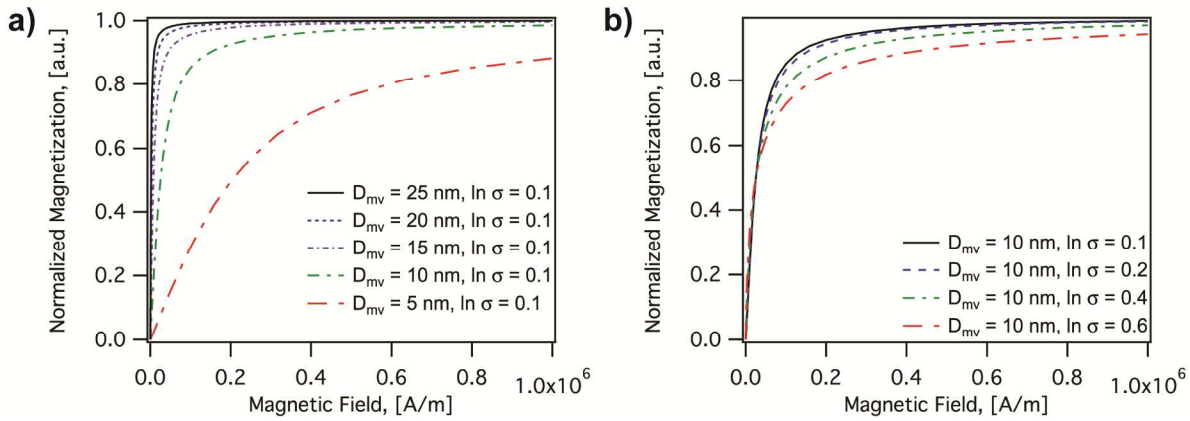

Figure S1. Calculated equilibrium magnetization curves based on the Langevin function weighted by a lognormal size distribution for a range of volume-median magnetic diameters and geometric deviations of the magnetic size distribution.

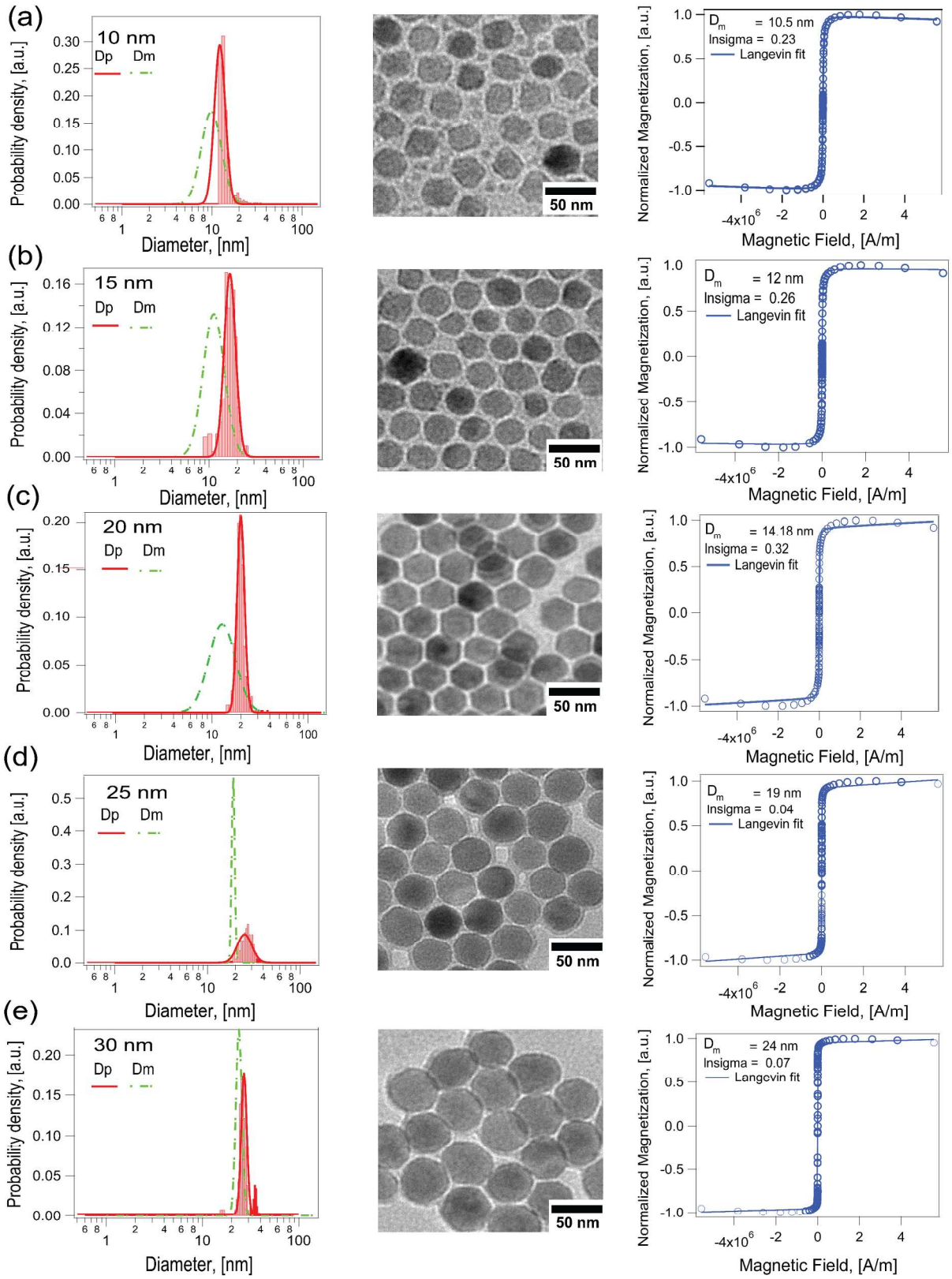

Figure S2. Representative TEM images, equilibrium magnetization measurements, and corresponding physical and magnetic size distributions for commercial obtained from Ocean

nanotech. The nominal diameters of (a) 10 nm (b) 15 nm (c) 20 nm (d) 25 nm (e) 30 nm correspond to the supplier's advertised size.

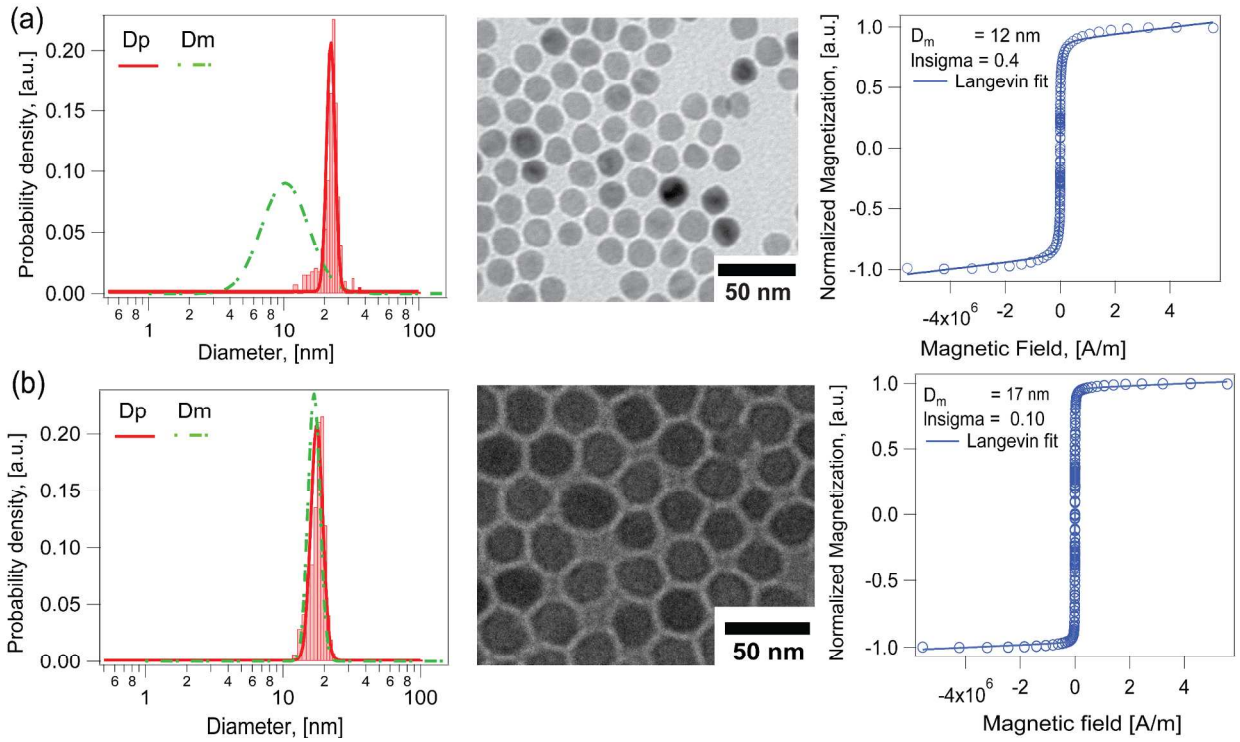

Figure S3. Representative TEM images, equilibrium magnetization measurements, and corresponding physical and magnetic diameter distributions for particles synthesized in the (a) absence and (b) presence of O_2 corresponding to Fig. 8, 10 and 11 in the manuscript.

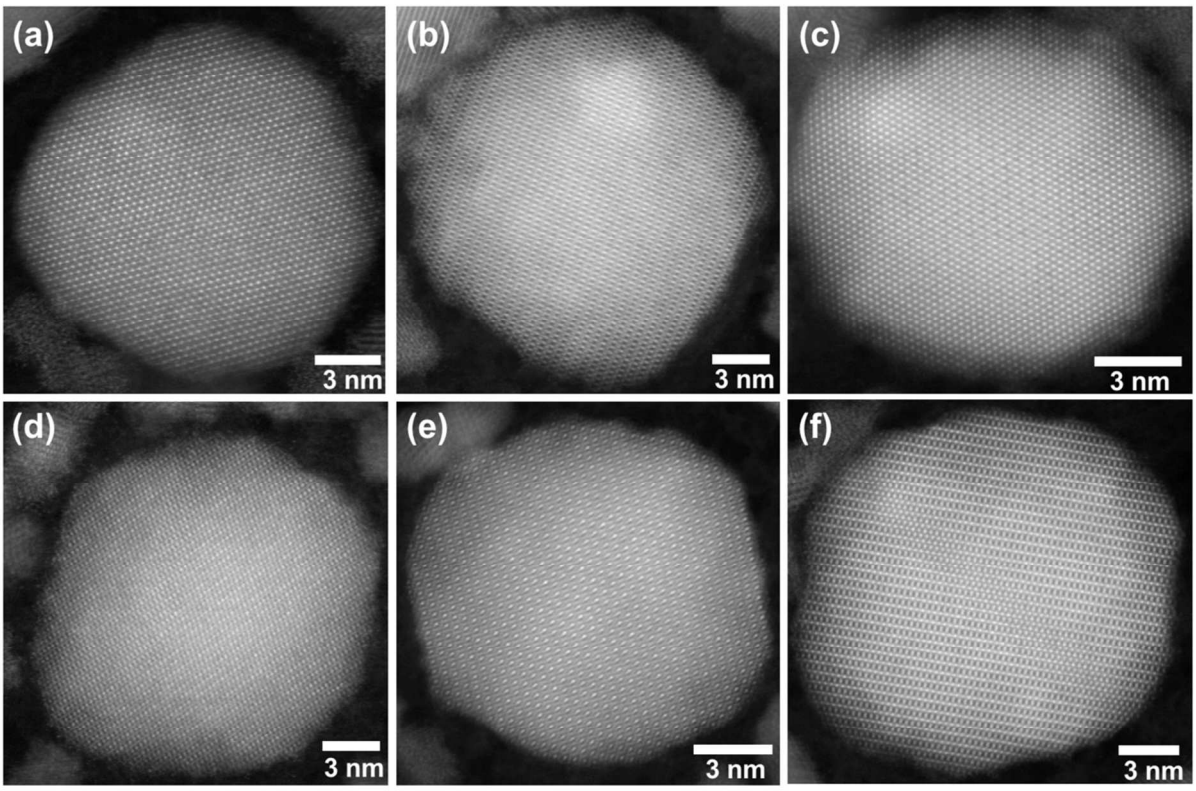

Figure S4. Particles synthesized in the presence of oxygen examined under atomic resolution HAADF-STEM were predominantly single crystalline and defect free. However, the occasional defect was observed; for example, a particle containing an antiphase domain boundary is shown in (f).

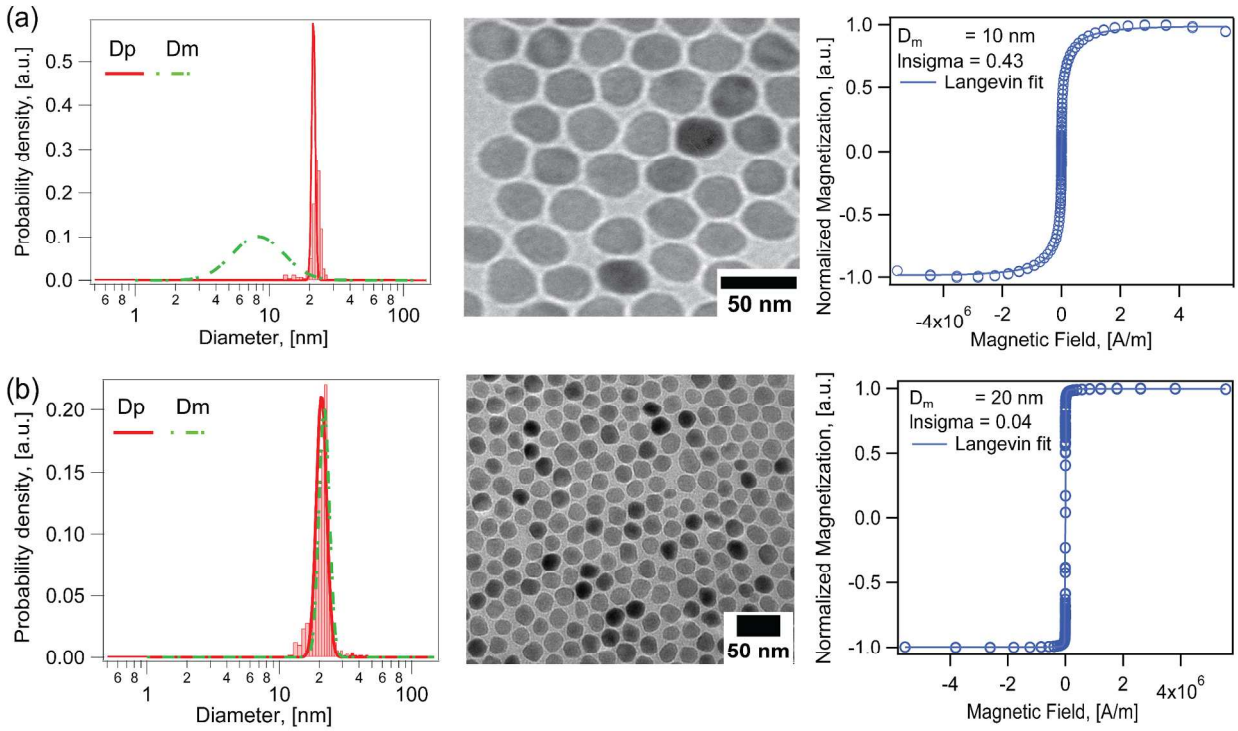

Figure S5. Representative TEM images, equilibrium magnetization measurements, and corresponding physical and magnetic diameter distributions for particles synthesized in the (a) absence and (b) presence of O_2 corresponding to Fig. 9 in the manuscript.

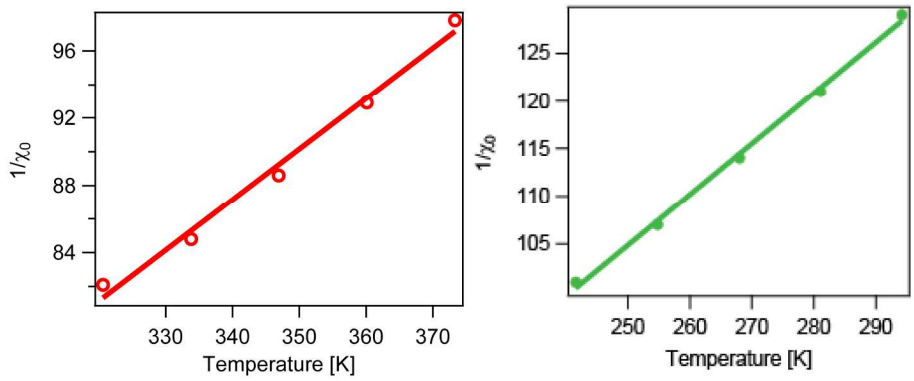

	D_p [nm]	sigma [nm]	D_m [nm]	sigma [nm]
W/O O_2	20	3	12	5
With O_2	18	1	17	2

Figure S6. Initial susceptibility measurements as a function of temperature used to calculate the interaction temperature parameter from the Curie Weiss law. Linear fit to $1/\chi_0$ vs T used to determine T_0.

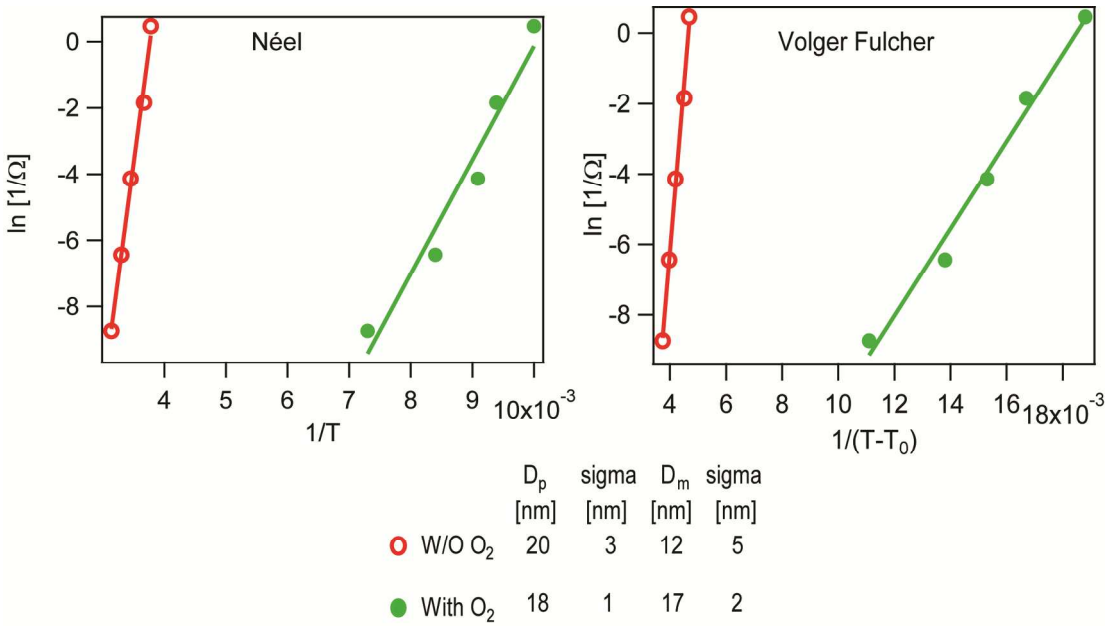

Figure S7. Analysis of ac susceptibility measurements as a function of temperature to obtain the magnetic anisotropy of nanoparticles synthesized in the presence and absence of oxygen. Plots of the natural logarithm of the inverse frequency as a function of the inverse of peak temperature, where the slope provides an estimate of the magnetic anisotropy energy and the y-axis intercept provides an estimate of τ_0 based

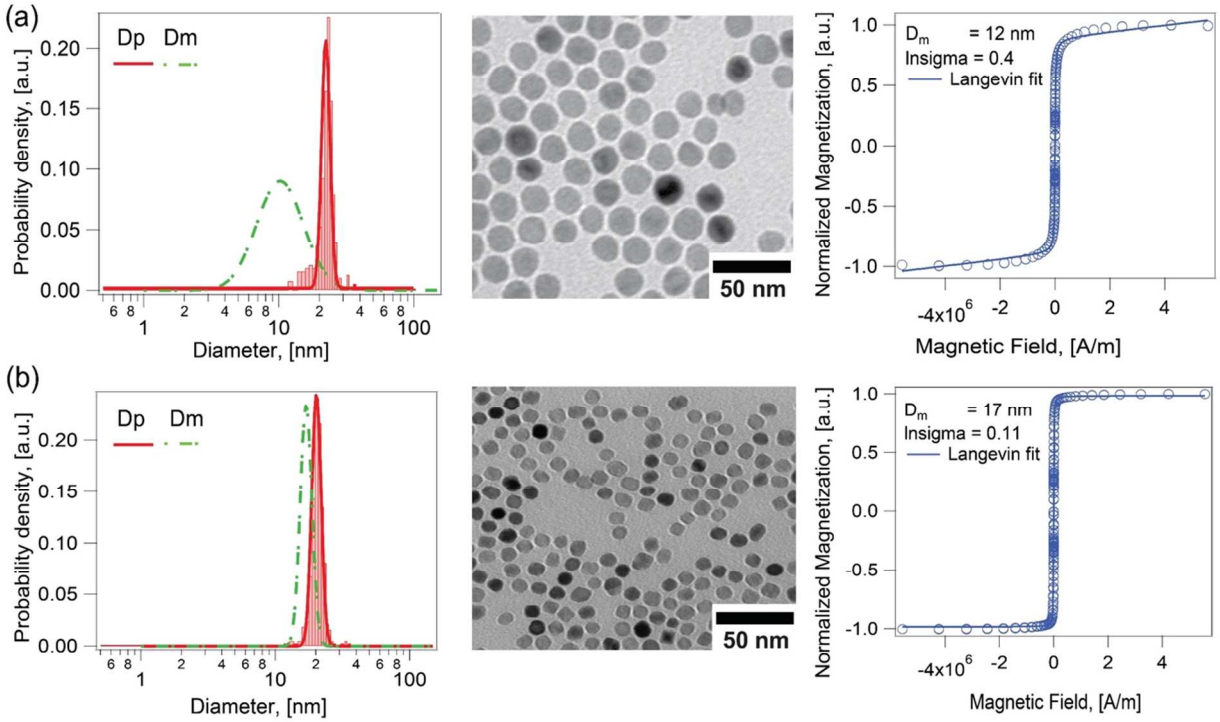

Figure S8. Representative TEM images, equilibrium magnetization measurements, and corresponding physical and magnetic diameter distributions for particles synthesized in the a) absence and b) presence of oxygen and coated with poly(ethylene glycol) (PEG) corresponding to Fig.13 and 14 in the manuscript.

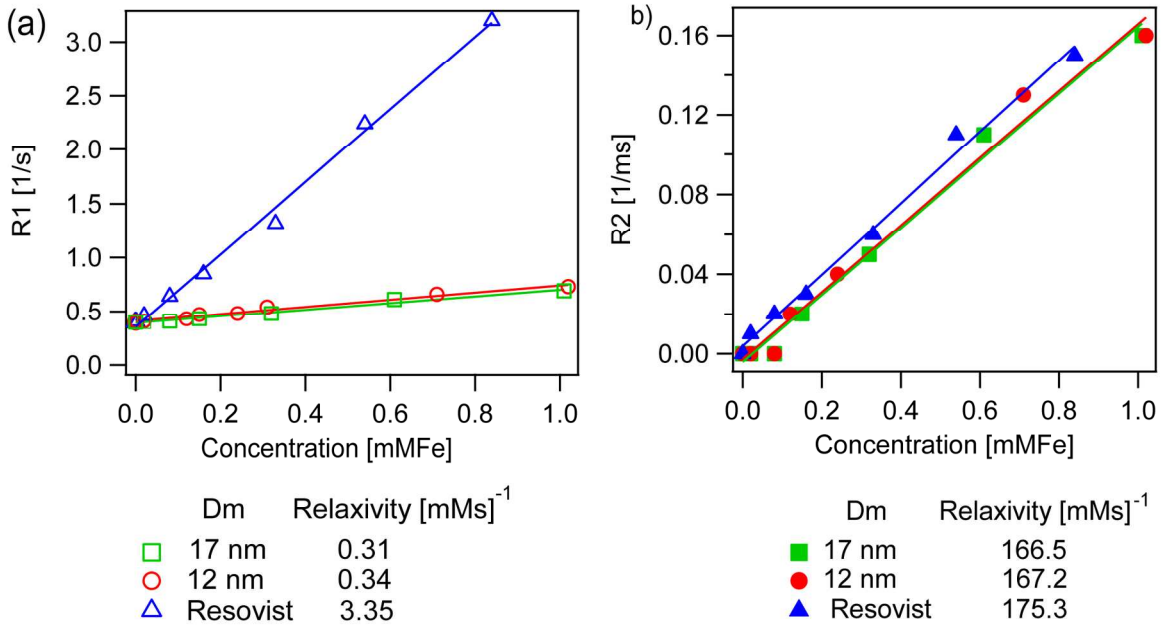

Figure S9. Longitudinal and transverse relaxivity measurements for particles synthesized in the presence and absence of oxygen, compared to the ferucarbotran (Resovist) particles. a) R1 and b) R2 relaxivities as a function of concentration compared for particles with magnetic diameter of 17 nm (synthesized with O_2), 12 nm (synthesized without O_2) and ferucarbotran (Resovist) particles

Table S1: Arithmetic volume mean diameter and arithmetic standard deviation of the physical and the magnetic diameters of nanoparticles obtained under various inert gases in the presence and absence of oxygen for the Extended LaMer (EL) and the heating up (Hp) thermal decomposition syntheses.

				Physical Diameter [nm]		**Magnetic Diameter[nm]**	
Synthesis	**Inert Gas**	**O_2 source**	**Time (hrs)**	**Arithmetic Volume Mean**	**Arithmetic Standard Deviation**	**Arithmetic Volume Mean**	**Arithmetic Standard Deviation**
Hp_Without Oxygen	N_2	-	1	18.31	1.10	10.71	5.58
Hp_With Oxygen	N_2	N_2/O_2	1	15.35	1.85	14.10	1.70
EL_Without Oxygen	Ar	-	2	18.43	1.11	10.05	5.00
			3	21.37	0.64	10.99	5.02
			4	24.62	1.73	13.28	6.29
			5	26.37	1.32	15.77	5.11
EL_Without Oxygen	N_2	-	2	18.99	3.41	15.37	3.42
			3	20.45	1.64	17.02	0.78
			4	24.06	3.87	18.01	0.72
			5	25.46	3.32	20.02	0.80
EL_With Oxygen	Ar	N_2/O_2	2	14.38	2.90	13.38	1.71
			3	16.58	3.69	14.50	1.02
			4	16.23	2.45	15.51	0.62
			5	17.08	2.23	16.01	0.64
EL_with Oxygen	Ar	Ar/O_2	2	19.23	2.34	16.71	0.67
			3	23.83	4.57	20.02	0.80
			4	22.63	2.04	22.02	0.88
			5	25.76	4.67	23.00	0.46
EL_with Oxygen*	Ar	Ar/O_2	2	13.62	2.61	13.24	2.54
			3	16.28	2.29	14.14	1.99
			4	17.50	2.82	16.10	1.78
			5	18.28	2.71	17.09	1.71

Except for *, all particles synthesized had oxygen addition from the start of precursor addition when docosane in the reactor had reached 350°C. In synthesis *, oxygen was added from the beginning of the synthesis when docosane was being heated up to 350°C.

Table S2: Comparison of the coercive fields and the remanent magnetization of particles synthesized with and without oxygen for two cycles of Field Cooling and Zerofield Cooling

		Hc_1 (A/m)	Hc_2 (A/m)	Mr_1 (Am^2/kg)	Mr_2 (Am^2/kg)
FC-Cycle 1	Without O_2	-35,524	26,394	73	-78
	With O_2	-19,265	19,073	50	49
FC-Cycle 2	Without O_2	-32,314	26,091	67	-58
	With O_2	-19,191	19,005	49	49
ZFC-Cycle 1	Without O_2	-31,970	26,057	67	-77
	With O_2	-19,101	19,100	49	49
ZFC-Cycle 2	Without O_2	-31,623	25,804	66	-57
	With O_2	-19,133	19,062	49	49

II. Safety Considerations for Safe Addition of Oxygen During Thermal Decomposition Synthesis

The stoichiometric rate of pure oxygen that was added as a reactive species for a given precursor addition rate during reaction was calculated using Table S3.

Table S3: Stoichiometric oxygen addition to a synthesis under an inert atmosphere

Iron concentration in precursor (mmol/ml)	0.22
Oleic acid concentration in precursor solution (mmol/ml):	1.11
Drip rate of precursor (ml/hr):	9
Time of reaction (hr):	6
Solution added to reactor (ml):	54
Iron (Fe) added (mmol) :	11.88
Total amount of oxygen required to oxidize iron to Fe_3O_4 (mmol) :	7.92
Molar flow rate of oxygen (mmol/s):	0.00037
Total mass of oxygen added to reactor (g):	0.25
Mass flow rate of oxygen (g/hr)	0.042
Volume of oxygen (cm^3) :	177.5
Flow rate of oxygen (cm^3/hr):	29.58
Molar fraction of oxygen in mixed feed	0.2
Flow rate of mixed feed (sccm):	2.34

Oxygen concentrations in the total gas flow supplied to the reactor were maintained below 5% and we did not observe any flashing or flames during any of the reactions. The choice of this value was based on a survey of reported limiting oxygen concentration (LOC) values for other organic vapors. However, it must be noted that information on LOC values at elevated temperatures is very limited and there are no direct measurements of LOC for the vapor mixture in the reactor. We therefore supplemented this safety measure with calculations of the maximum rates of combustion of the various components, based on the idea that oxygen would be the

limiting reactant. The molar heats of combustion for each of the organic vapors were calculated to estimate the rate of heat evolved per mole of oxygen assuming combustion under the reaction conditions. Calculations were based on using the Hess Law and the stoichiometry of the combustion reactions for each of the solvents, as given in Table S4.

Table S4: Calculated heats of combustion and rates of heat generation for solvents.

Compound	**Combustion reaction**	**Heat of combustion, per mole O_2, 350 °C (kJ/mol)**	**Rate of heat generation (J/s)**
Docosane	$C_{22}H_{46} + 33.5O_2 \rightarrow 22CO_2 + 23H_2O$	-320.47	0.47
Oleic acid	$C_{18}H_{34}O_2 + 25.5O_2 \rightarrow 18CO_2 + 17H_2O$	-315.66	0.47
1-Octadecene	$C_{18}H_{34} + 26.5O_2 \rightarrow 18CO_2 + 17H_2O$	-308.25	0.46

The expected temperature rise rates assuming each of the solvents were to combust individually with oxygen entering the reactor were calculated based on the rates of heat generation in Table S4 and the masses and heat capacities of the contents of the reactor are plotted in Fig. S10. Temperature rise rates were estimated to be of the order of 0.002 °C/s at the start of the reaction and decreased continuously with time because of the increasing volume of the reactant mixture, which translates to a larger thermal mass. Based on this expected rate of temperature rise, we concluded that if combustion were to occur, it would not be difficult to control, as long as the overall rate of oxygen addition is controlled. Still, reactions were continuously monitored for evidence of flashes and for sudden temperature rises with the idea that if these were observed we would immediately shut off oxygen addition. Fortunately, this was not the case in any of the experiments reported here.

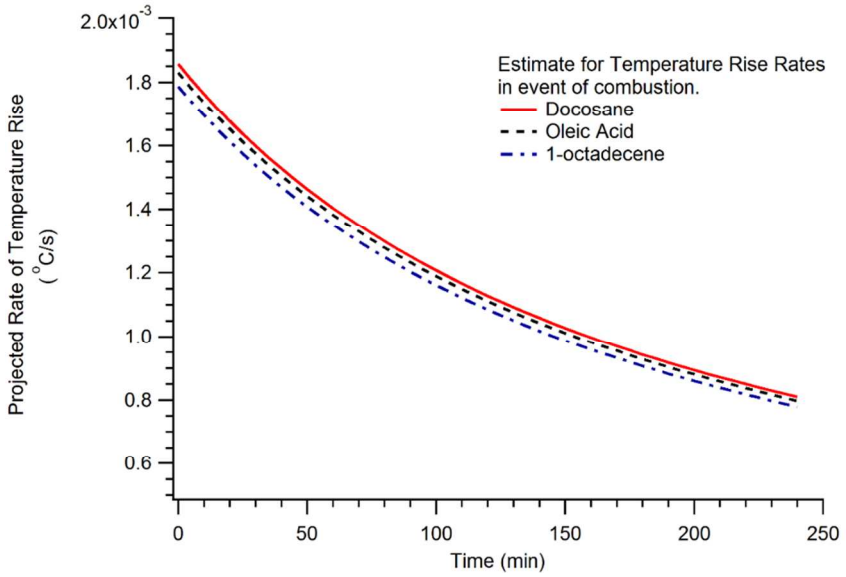

Figure S10. Calculated rates of temperature rise during the reaction. The rates are calculated assuming combustion of each solvent with the oxygen entering the reactor.